SCIENTIFIC REPORTS

OPEN

SUBJECT AREAS:
COMPUTATIONAL CHEMISTRY
CHEMICAL PHYSICS

Received
14 May 2014

Accepted
2 July 2014

Published
25 July 2014

Correspondence and requests for materials should be addressed to K.S.K. (kimks@unist.ac.kr)

* These authors contributed equally to this work.

Anisotropic Charge Distribution and Anisotropic van der Waals Radius Leading to Intriguing Anisotropic Noncovalent Interactions

Hahn Kim[1]*, Van Dung Doan[2]*, Woo Jong Cho[3], Miriyala Vijay Madhav[2] & Kwang S. Kim[3]

[1]Department of Chemistry, Korea Advanced Institute of Science and Technology, Daejeon 305-701, Korea, [2]Department of Chemistry, Pohang University of Science and Technology, Pohang 790-784, Korea, [3]Department of Chemistry, School of Natural Science, Ulsan National Institute of Science and Technology (UNIST), Ulsan 689-798, Korea.

Although group (IV–VII) nonmetallic elements do not favor interacting with anionic species, there are counterexamples including the halogen bond. Such binding is known to be related to the charge deficiency because of the adjacent atom's electron withdrawing effect, which creates σ/π-holes at the bond-ends. However, a completely opposite behavior is exhibited by N_2 and O_2, which have electrostatically positive/negative character around cylindrical-bond-surface/bond-ends. Inspired by this, here we elucidate the unusual features and origin of the anisotropic noncovalent interactions in the ground and excited states of the 2nd and 3rd row elements belonging to groups IV–VII. The anisotropy in charge distributions and van der Waals radii of atoms in such molecular systems are scrutinized. This provides an understanding of their unusual molecular configuration, binding and recognition modes involved in new types of molecular assembling and engineering. This work would lead to the design of intriguing molecular systems exploiting anisotropic noncovalent interactions.

Molecular recognition and self-assembly of biomolecules and nanomaterials[1–4] are governed mostly by non-covalent interactions[5–7] including hydrogen bonding[8–10], π-interactions[11–15], and halogen bonding[16–22]. Quite often, molecular conformations are determined by electrostatic interactions which are generally described by isotropic atomic charges. However, atomic charges in molecules are not isotropic. As a simple example, the σ_g molecular orbital (MO) of an H_2 molecule shows overlap between 1s atomic orbitals (AOs) of the two atoms. This overlap increases the electron density (ρ_e) between the two nuclei (i.e., over the cylindrical surface surrounding the bond), which results in negative electrostatic potential (ESP). Then, the decreased ρ_e outside the two nuclei (around bond-ends) results in positive ESP. Thus, the quadrupole moment (Q_{zz}) for the case where the two atoms are along the z-axis is positive (0.45 debye·Å). Such phenomena could be expected for all the homonuclear diatomic molecules regardless of the σ- or π-type overlap, as can be seen from ESP maps of H_2 (σ_g MO) and C_2 (π_u MO) shown in Figure 1a. The anisotropic charge distributions result in highly direction-specific interactions best exemplified by halogen bonding, the origin of which is generally explained by the concept of σ-hole[23–27]. This anisotropy in charge distribution is visualized in F_2 and Cl_2 ESP maps (Figure 1a). It can be understood as a "hole" residing in the antibonding σ*-orbital. Since this σ-hole, in principle, forms at both ends of every σ-bond, one might expect that this concept would be applicable to all the elements.

In this regard, we have calculated the ESP maps for homonuclear diatomic molecules of second and third row elements. We note that, for N_2 and O_2, the covering of σ-hole by the nonbonding electrons inverts the typical anisotropy (Figure 1a). N_2 shows negative ESP at bond-ends and positive ESP around the cylindrical-bond-surface. A similar result was also reported very recently by Hobza and coworkers[28]. A simple AO-overlap concept cannot explain the N_2 case. The positive ESP around the cylindrical-bond-surface between two N nuclei of the N≡N bond is even more difficult to understand, since compounds with C≡C bonds usually undergo facile reactions with electrophiles[29].

To understand this puzzling anomaly, we investigated the difference in MOs and natural bonding orbitals (NBOs) for the ground states of N_2, $^tO_2$, F_2, P_2, $^tS_2$, and Cl_2 and their first excited states ($^tN_2$, O_2, $^tF_2$. $^tP_2$, S_2, and

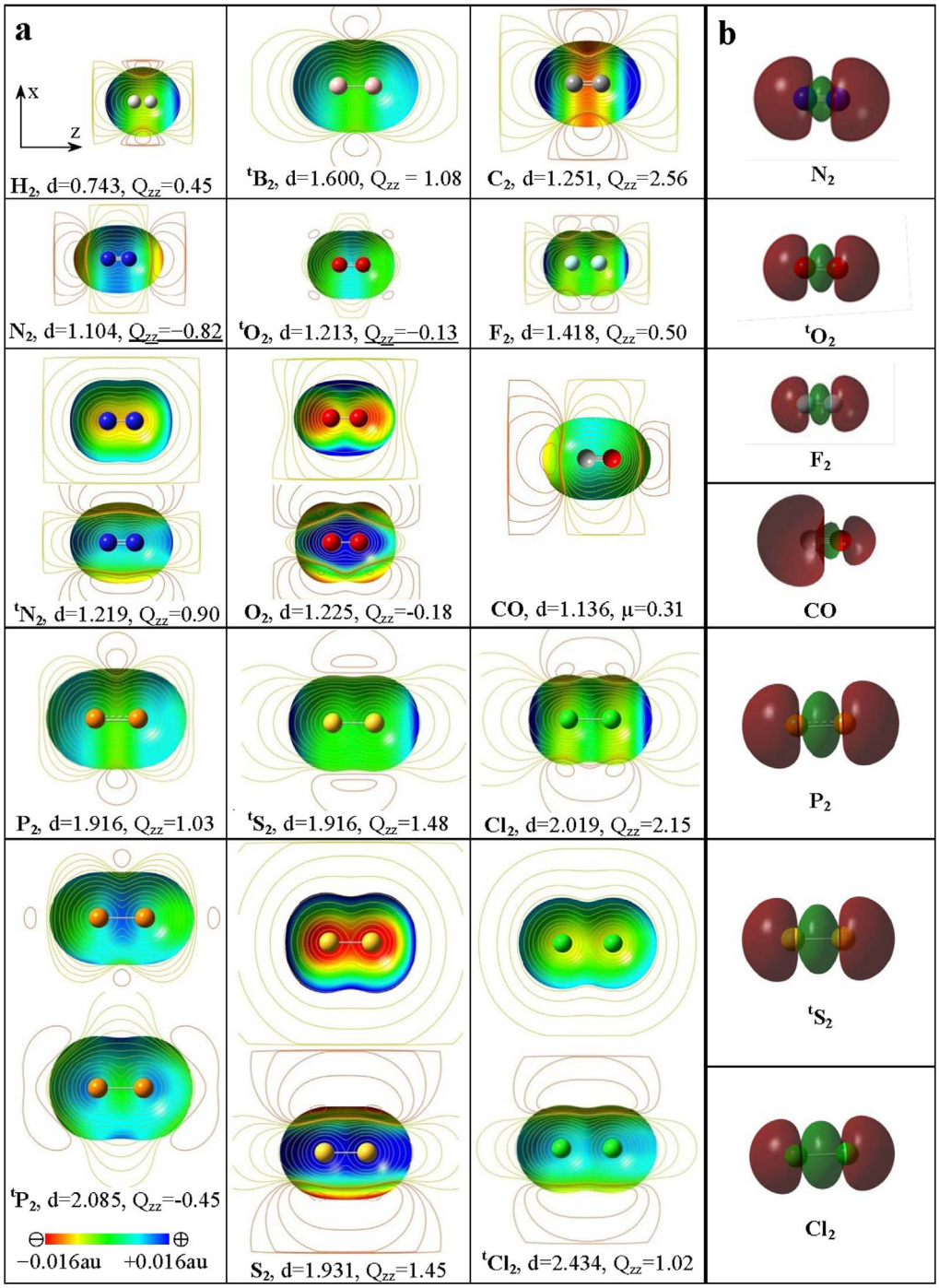

Figure 1 | ESP maps and σ-bonding valence MO. (a). Ground/first excited states of A_2 (A: N, O, F, P, S, Cl) at the MP2/aVTZ level of theory (density isovalue: 0.001 au.). H_2, B_2, C_2, CO (isoelectronic to N_2) are added for comparison. Superscript "t" means triplet state. The Be_2 and $^tF_2$ are not drawn because of dissociation at the CCSD(T)/aVTZ level. The bond-length (d in Å), quadrupole moment (Q_{zz} in debye · Å), and dipole moment (μ in debye) are given at the optimized CCSD(T)/aVTZ geometry. (b). σ-bonding orbitals of the ground-state structures.

$^tCl_2$), where the superscript "t" denotes triplet-state. The differences in orbital hybridization, bond-length, and nuclear-charge turn out to be important factors in anisotropy. To investigate the anisotropy effect on the measurable quantities, we studied the interaction of homonuclear diatomic molecules with themselves, positively/negatively charged ions (Na^+, Cl^-), a water molecule and a benzene molecule, using Møller-Plesset second-order perturbation theory (MP2) and coupled-cluster theory of singles, doubles and perturbative triples excitations (CCSD(T)) at the complete basis set (CBS) limit. Here we discuss the anomaly arising from the charge anisotropy of N_2 and $^tO_2$ in particular.

Results

Ground states of N_2, $^tO_2$ and F_2. ESP contour maps of representative homonuclear diatomic molecules at their optimized geometries are shown in Figure 1a along with their bond distance (d) and Q_{zz}. Inspection of the Q_{zz} values of second-row homonuclear diatomic molecules ($^tB_2$, C_2, N_2, $^tO_2$, F_2) reveals that Q_{zz} decreases abruptly to a negative value at N_2, and again increases to a positive value at F_2. This sign change in Q_{zz} indicates the inversion of anisotropy at N_2. Consistent to this observation, the ESPs of N_2 and $^tO_2$ are negative at bond-ends and positive around the cylindrical-bond-surface, unlike other ground state species. The

issue of Q_{zz} and its relation to ESP was also addressed in literature recently[28,30].

To find a qualitative reasoning for the prominent difference between N_2 and F_2, we take both ρ_e and nuclear charge into account. Nitrogen has a smaller effective nuclear-charge ($Z_{eff}(N_{2p}) = 3.83$) than fluorine ($Z_{eff}(F_{2p}) = 5.10$)[31]. Therefore, at some distances from the bond-ends the $\rho_e(N)$ becomes higher than $\rho_e(F)$, as can be seen from the σ-bonding MOs shown in Figure 1b. Furthermore, since the bond length of N_2 (1.10 Å) is much shorter than that of F_2 (1.42 Å), the large electron-population required by the N≡N triple bond cannot be accommodated within such a small space between the two N nuclei. A nodal plane bounded by a positively charged region near each nucleus and a negatively charged region somewhat away from the N nucleus is formed outside each N nucleus. This is because a large fraction of electron-population in a large space outside the N nucleus (though not dense) screens out the small effective positive charge of the N nucleus beyond a certain distance from the nucleus. As a result, a small portion of the total electron-population in the N≡N bond and the summed nuclear-charge of two closely adjacent N nuclei make the cylindrical-bond-surface electrostatically positive. In contrast, a small electron-population of the F-F single bond can be easily accommodated in a reasonably large space between the two F nuclei. In F_2, a large fraction of the total electron-population stays around the bond-ends, whereas only a small portion of the total electron-population stays outside the two F nuclei. Therefore, the regions outside the F-F bond-ends are positively charged due to the large nuclear-charge and small electron-population, whereas the cylindrical-bond-surface between the two F nuclei is negatively charged due to the large fraction of electron-population. In the case of the ground triplet state $^tO_2$, its molecular size and electronic properties are between those of N_2 and F_2, as visualized from their σ-bonding MOs (Figure 1b). The bond-ends are nearly neutrally charged or very weakly positively charged. Even though the effective charge of O ($Z_{eff}(O_{2p}) = 4.45$) is almost in between those of N and F, the $^tO_2$ double-bond-length (1.21 Å) is still short, closer to the bond-length of N_2 than F_2, and so the cylindrical-bond-surface of $^tO_2$ is still positively charged, and its bond-ends are nearly neutral but weakly electrostatically negative. The most electrostatically positive site is the flat potential region $-60^\circ < \theta < 60^\circ$ around the O nucleus.

To explain in a more quantitative manner, we computed the NBOs of N_2, $^tO_2$, F_2 and their third-period analogues. From the s-p hybridization characters of σ-lone pairs lying on the bond axis, we find an important difference in p-character among the lone pairs on N_2 (37%), O_2 (18%) and F_2 (5%) (Supplementary Table S1), which is due to the bond-length, the energy-gap between s and p orbitals, and nuclear-charge. For this reason, the 2s-electrons of N atoms spill out of the bonding region upon the formation of N_2, making bond-ends negatively charged. On the other hand, the 2s-electrons (95%) of F atoms stay localized upon the formation of F_2 (not compensating for the σ-holes at bond-ends), making bond-ends positively charged. The charge anisotropy of $^tO_2$ lies in between those of N_2 and F_2, featuring a near-flat ESP on the density isosurface. As for a large nuclear-charge, the s-orbital is favored in order to screen the nuclear-charge but not sufficient enough, giving positive ESP around the bond-ends. For a small nuclear-charge, the somewhat p-like electron-population can be widely dispersed, resulting in negative ESP due to the still significant ρ_e in the bond-ends. This can be seen from the ESP map of CO (isoelectronic to N_2), where the electron-population around the C atom is dispersed, while that around the O atom is highly contracted, as noted from the HOMO of CO in Figure 1b.

Ground states of P_2, $^tS_2$ and Cl_2. The anisotropy of ESP of the third-period equivalents is less prominent than their second-period equivalents. Owing to the increased bond-length, the ESP is negative near the mid-region of the cylindrical-bond-surface because the effect of two nuclear-charges is sub-additive. The lengthening of bonds also leads to the decrease in 3s-3p orbital mixing, resulting in the localization of σ-lone pairs in 3s-orbitals. For example, the bond length of Cl_2 (1.99 Å) is longer than that of F_2. Its bond-ends are more positively charged than that of F_2, but the overall pattern of ESP is alike. Analogously, one could expect that the ESP of the triplet ground state $^tS_2$ is also similar to that of $^tO_2$. However, since the S = S bond-length (1.90 Å) is much longer than that of $^tO_2$ (1.21 Å), the ESP contribution from the two nuclei is rather weak at the mid region of the cylindrical-bond-surface of $^tS_2$. Therefore, the mid-region of $^tS_2$ is electrostatically negative unlike that of O_2, which in turn results in electron deficiency in the $^tS_2$ bond-ends. Overall, $^tS_2$ behaves rather similarly to F_2/Cl_2. P_2 forms a triple-bond with one σ-bonding and two π-bonding MOs. However, the large internuclear separation (1.92 Å) makes the mid-bond highly electrostatically negative, thereby resulting in electrostatically positive bond-ends. Thus, P_2 behaves oppositely to N_2, but rather similarly to F_2/Cl_2 despite the fact that N and P belong to the same group V.

Excited States. The anisotropic ESPs of the excited states of homonuclear diatomic molecules are also shown in Figure 1a. ESP patterns of the excited states are in many cases opposite to the ground state. Such trends appear for the excited state of all other homonuclear diatomic molecules. Since the excited states show ESP patterns different from or opposite to the corresponding ground state, one can imagine laser-controlled on-off motion which can lead to the design of molecular flippers or nanomechanical devices including molecular switches[32].

We consider the cases where N_2, $^tO_2$ and F_2 are excited to triplet, singlet and triplet states, respectively. The excited triplet $^tN_2$ has one σ_g bonding, one π_{ux} bonding, one half-occupied π_{uy} bonding and one half-occupied π_{uy}* antibonding. Since one of the π bonds is lost upon excitation, the bond distance is lengthened to 1.22 Å. As such, the electron-population between two N nuclei in $^tN_2$ no longer spills over outside the N nuclei, in contrast to the overcrowded electron-population between the two closely bound N nuclei in the ground singlet N_2. The large electron-population between two N nuclei in the π_{uy} MO cancels the depleted electron-population in the π_{uy}* MO. Additionally, the σ_g bonding makes the bond-ends electrostatically positive along the z-axis by the overlap between the two p_z orbitals. On the other hand, the π_{ux} MO induces negative ESP due to highly increased ρ_e on the top and bottom of the cylindrical-bond-surface (top view of $^tN_2$ in Figure 1a), while it introduces positive ESP due to the depleted ρ_e on the front and back of the cylindrical surface (bottom front view of $^tN_2$ in Figure 1a). The effective MOs for $^tN_2$ are a half σ_g bond, one π_{ux} bond and a half π_{uy} bond. In the case of the singlet O_2, one σ_g bond, two π_u bonds, and one π_g* bond (the effective MOs: one σ_g bond, one π_{ux} bond) behave similarly as in the N_2 case. Also, in the case of the singlet F_2, one σ_g bond, two π_u bonds, one and a half π_g* bond and a half σ_u* bond behave similarly as in the N_2 case. This is explained by cancellation between bonding and antibonding such that the resulting effective MOs are a half σ_g bond and a half π_u bond, which is similar to the singlet O_2 and the triplet $^tN_2$. The excited states $^tP_2$, S_2, and $^tCl_2$ show similar trends, as discussed for $^tN_2$ and O_2. In the $^tP_2$ case, the contrast between the maximum and minimum ESP is slightly weaker than in S_2 and $^tCl_2$.

Even when an electron is fully excited to a cationic state, the anisotropic charge distribution can still be seen though the polarization effect is diminished by the charge effect. The discussion along with the ESPs of ionized homonuclear diatomic molecules and the issues of MO energy level diagrams[31,33] for the charged states is in Supplemenatry note 1.

van der Waals atomic radii in homodiatomic molecules. In molecular interactions the electrostatic interactions (E_{el}) often govern molecular structures. The van der Waals interactions composed of the dispersion energies (E_{disp}) and exchange repulsion energies (E_{exch}) determine molecular size. The van der Waals radii of atoms

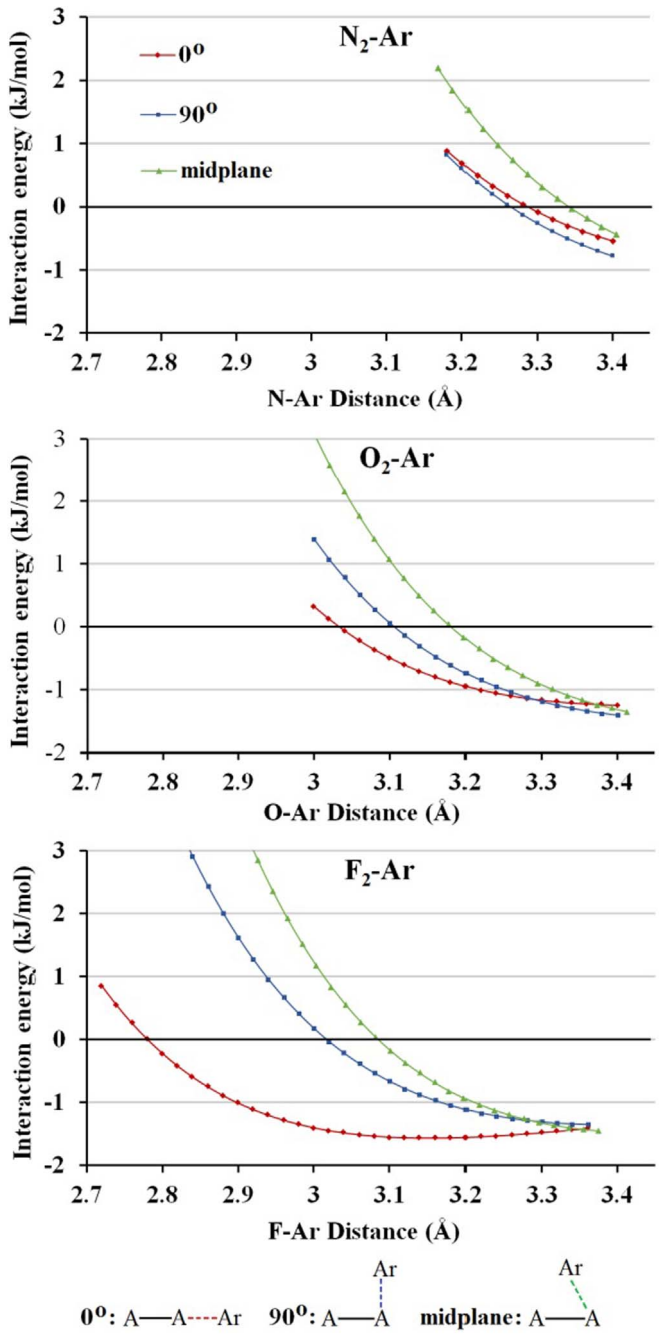

Figure 2 | Anisotropic hard wall distance (Å) of an atom N/O/F in the molecule $N_2/O_2/F_2$ for three different orientations (0°, 90°, central): N (3.29, 3.26, 3.34), O (3.03, 3.11, 3.18), F (2.78, 3.02, 3.08) at the CCSD(T)/CBS level (see text for van der Waals radius).

are generally treated isotropically because their features are considered to be hardly susceptible to the environmental effects. Nevertheless, we note a significant anisotropy in van der Waals radius (r_v) of each atom in N_2, $^tO_2$ and F_2, namely, a significant difference among the $\theta = 0^\circ$ direction (atoms end), the $\theta = 90^\circ$ direction, and the central direction from a nucleus to the plane bisecting two nuclei (Figure 2). By excluding the hard wall radius (r_w) of Ar (1.685 Å), the r_w values (in Å) for the cases of $\theta = 0^\circ/\theta = 90^\circ$/central are 1.60/1.58/1.66 for N_2, 1.35/1.42/1.50 for $^tO_2$, and 1.10/1.33/1.40 for F_2, and their van der Waals radii (r_v) are considered to be $1.122(=2^{1/6})$ times that of the r_w. The r_w decreases moving right in the periodic table from N_2 to F_2. The r_w changes depending on orientation angles, showing anisotropic behavior. The r_w(central) is the largest, while the $r_w(\theta = 0^\circ)$ tends to have a smaller value. It is because overall the cylindrical-bond-surface has much denser electron-population due to two adjacent positively charged nuclei, while the bond-ends have less dense and diffuse electron-population. In the case of N_2 the $r_w(\theta = 0^\circ)$ is similar to but slightly larger than $r_w(\theta = 90^\circ)$ because of significantly large electron-population along the bond-ends. F_2 shows much more anisotropic behavior in the van der Waals radius in that the $r_w(\theta = 0^\circ)$ is much smaller than the r_w(central), which reflects the σ-hole effect. The angular dependence of the size of the atom was experimentally noted and theoretically described within halogen bonding in terms of polar flattening[34–36].

Interactions of homonuclear diatomic molecules with ionic species Na^+ and Cl^-. Physical manifestation of the ESP maps can be understood by considering the interaction energy between homonuclear diatomic molecules with a positively or negatively charged ion (Na^+ or Cl^-) (Figure 3). The bond-ends of N_2 favor cationic species, whereas those of $F_2/Cl_2/^tS_2$ favor anionic species. $^tO_2$ favors cationic species at bond-ends, but behaves somewhat isotropically towards anionic species. P_2 behaves nearly isotropically towards cationic species, but strongly favors the $\theta = \pm 60^\circ$ direction towards anionic species.

N_2 strongly interacts with Na^+ around the bond-ends (interaction energy $E_e = -30$ kJ/mol at the distance from the ion to the nearest nucleus (d_n) of 2.53 Å according to the CCSD(T)/CBS energy and CCSD(T)/aVTZ optimized geometry. In contrast, F_2 strongly interacts with Na^+ around the cylindrical mid-surfaces of the bond ($E_e = -14$ kJ/mol) at the distance from the ion to midpoint of the two nuclei (d_m) of 2.54 Å. $^tO_2$ behaves between N_2 and F_2, but slightly more closely to N_2, because Na^+ favors the bond-ends of $^tO_2$ ($E_e = -16$ kJ/mol, $d_n = 2.57$ Å). P_2 shows almost isotropic potential ($E_e = -37$ kJ/mol at $d_m = 3.05$ Å; $E_e = -34$ kJ/mol at $d_n = 2.98$ Å). $^tS_2$ strongly favors Na^+ around the cylindrical mid-surfaces of the bond ($E_e = -34$ kJ/mol at $d_m = 2.91$ Å; $E_e = -18$ kJ/mol at $d_n = 2.92$ Å). Cl_2 shows $E_e = -34$ kJ/mol on the cylindrical mid surface ($d_m = 2.76$ Å), but no binding along the z axis.

On the other hand, for Cl^-, N_2 strongly interacts with it around the mid-point of the cylindrical-bond-surface ($E_e = -9$ kJ/mol at $d_m = 3.55$ Å); in contrast, F_2 strongly interacts along the bond-ends along the z axis ($E_e = -90$ kJ/mol, $d_n = 1.95$ Å). $^tO_2$ behaves almost in between N_2 and F_2, but again slightly more closely to N_2, because the cylindrical-bond-surface is more favored ($E_e = -6$ kJ/mol at $d_m = 3.57$ Å; $E_e = -5$ kJ/mol at $d_n = 3.40$ Å). P_2 shows the strongest interaction ($E_e = -62$ kJ/mol) at the distance from the mid-point of a molecule to an ion around $\theta = 60^\circ$ from each nucleus ($d_{m'}$) (3.07 Å). $^tS_2$ gives $E_e = -40$ kJ/mol at the bond-ends ($d_n = 2.97$ Å), and Cl_2 shows $E_e = -102$ kJ/mol at the bond-ends ($d_n = 2.33$ Å). As such, we confirmed that the interaction of homonuclear diatomic species with closed-shell ions is mainly determined by the ESP of the diatomic species.

Interactions of the homodiatomic molecules with H_2O. Water moisture is present in air, which is composed predominantly of N_2 and O_2. In clouds, on wet surfaces, and on the surface of water in rivers, lakes, and sea, the water molecules and clusters interact with N_2 and O_2 in the atmosphere. Even though individual interaction is small in magnitude, their abundance in the huge atmospheric space on earth is enormous. For this reason, understanding their accurate interactions is highly important. Figure 4a shows the interactions of H_2O with N_2, $^tO_2$, O_2, and F_2. N_2 interacts strongly with the H of H_2O on the bond-ends (interaction energy $E_e = -5.17$ kJ/mol) and weakly with the O of H_2O on the cylindrical-bond-surface ($E_e = -2.96$ kJ/mol). However, in the case of F_2, the F-F bond-ends interact strongly with the O of H_2O ($E_e = -5.71$ kJ/mol), while the cylindrical-bond-surface interacts with the O of H_2O ($E_e = -4.70$ kJ/mol). In the cases of $^tO_2$, and O_2, the O at an edge of the

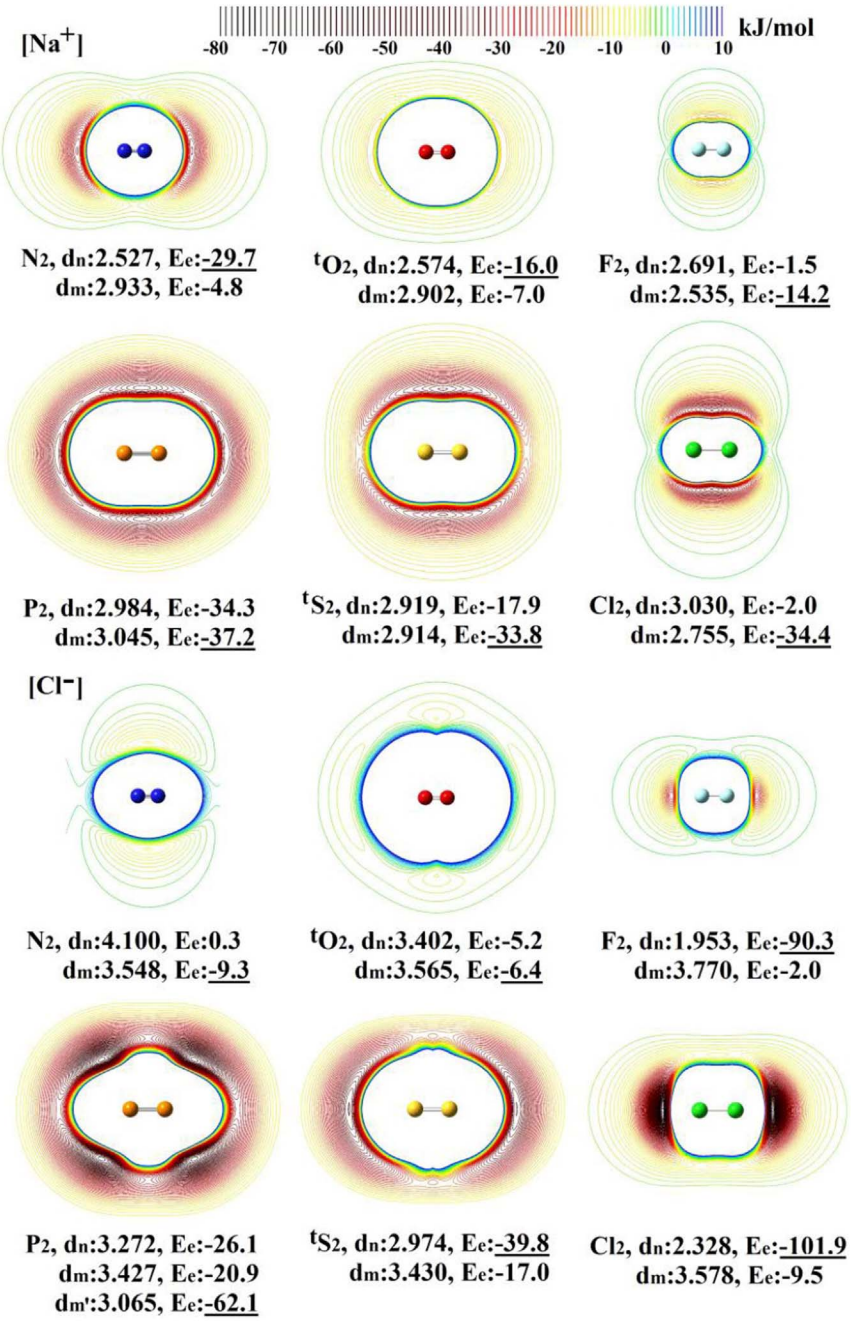

Figure 3 | Interactions of homodiatomic molecules with Na^+ (upper panel) and Cl^- (lower panel) calculated at MP2/aVTZ (contours at −80 to 10 kJ/mol), distance *d* in Å at CCSD(T)/aVTZ, and interaction energy E (E_e) in kJ/mol at CCSD(T)/CBS. d_n is the shortest distance from a nucleus to an ion in the linear structure; d_m is the distance from the mid-point of a molecule to an ion on a perpendicular position; $d_{m'}$ in Cl_2 is the distance from a nucleus to an ion along the θ = 60° direction. Superscript "t" means triplet state. The lowest MP2/aVTZ E_e in the contour map obtained with the fixed nuclei geometry of each free dimer is similar to the CCSD(T)/CBS E_e's at the CCSD(T)/aVTZ optimized geometry. An exception is F_2 for which the lowest MP2/aVTZ E_e in the contour map (for the fixed F-F bond-length 1.40 Å and the F…Cl distance 2.55 Å) is only −23 kJ/mol, but the fully optimized CCSD(T)/CBS E_e is −90 kJ/mol because the F-F distance is highly increased to1.84 Å and the F…Cl distance is drastically decreased to 1.95 Å like F^-…F-Cl).

cylindrical-bond-surface (making an angle of ~60° with respect to the z axis) interacts with H of H_2O (E_e = −2.33 kJ/mol and E_e = −6.37 kJ/mol, respectively). At the interface between water and the atmosphere, the H atoms in H_2O tend to interact strongly with the bond-ends of N_2, while the interaction with $^tO_2$ is somewhat weaker. Given that the O atoms in water are better stabilized by coordinating H atoms of other water molecules than the H atoms stabilized by O atoms of other water molecules, as noted in water clusters[37] and water surfaces[38,39], such interaction would help H atoms in the water surface interact with the bond-ends of N_2 molecules.

Interactions in homo-dimers and hetero-dimers of the homonuclear diatomic molecules. The structures of homo-dimers and hetero-dimers for the homonuclear diatomic molecules are shown in Figure 4b. Binding energies of these structures are governed by the electrostatic interaction and van der Waals interaction. Using

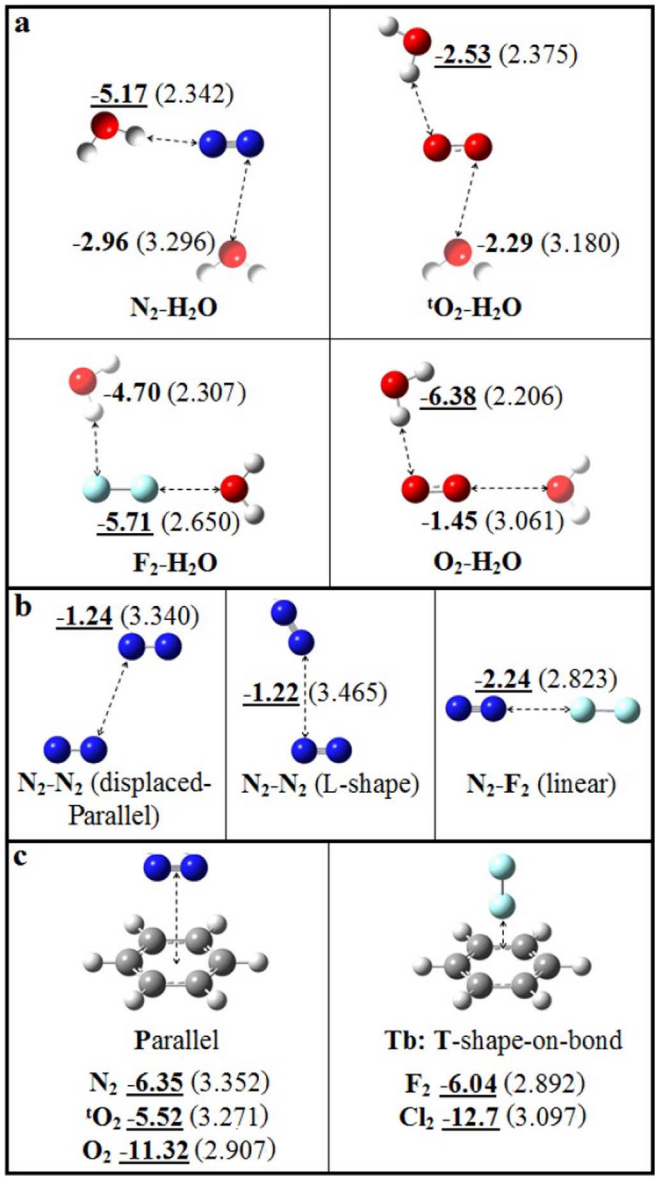

Figure 4 | Interactions of homonuclear dimers X_2 (or Y_2) with water, X_2/Y_2, and benzene. (a). Interaction of a single water molecule with $N_2/^1O_2/O_2/F_2$. The binding energies E_e are given for both the most stable structure interacting with H of a water molecule and that with O of a water molecule. For the less stable structure between the H and O interaction cases, the water molecule is given with a half-tone color. (b). Interactions of N_2 with N_2 and F_2. (c). Interactions for benzene-X_2 (X = N, ^{1}O, O, F, Cl). All binding energies E_e are given in kJ/mol at the CCSD(T)/CBS level. Each distance marked in a dotted line is given in Å (in parentheses) for the CCSD(T)/aVTZ optimized geometry (In the case of benzene-X_2, only the interacting distance was optimized at the CCSD(T)/aVTZ level using the BSSE-corrected MP2/aVTZ geometry).

symmetry adapted perturbation theory (SAPT)[40,41], we performed energy decomposition with the asymptotically corrected (AC) PBE0 functional and the aVTZ basis set on the MP2/aVTZ optimized geometry. We analyzed the SAPT interaction energy components [electrostatic energy (E_{es}), effective induction energy ($E_{ind*} = E_{ind} + E_{exch\text{-}ind}$), effective dispersion energy ($E_{disp*} = E_{disp} + E_{exch\text{-}disp}$), effective exchange repulsion (E_{exch*}: sum of the first order perturbation terms)[42], remaining higher order correction term (E_{HF}), and total SAPT interaction energy E_{tot}] (Supplementary Table S2). For most of the structures studied here, $|E_{disp}*|$ is much larger than $|E_{es}|$. In this case, E_{disp*} tends to be partly cancelled by E_{exch*} at the equilibrium structure except some special cases where $|E_{es}|$ is almost equivalent to or larger than $|E_{disp}*|$. Since $E_{exch}*$, $E_{disp}*$, and E_{es} are proportional to r^{-12}, r^{-6}, and r^{-1}, respectively, (where r is the interatomic distance), $E_{exch}*$ and $E_{disp}*$ which have sharp slopes with respect to r tend to be cancelled out to give an energy minimum point, while E_{es} showing a much weaker slope tends to change the minimum point slightly. This is the reason why E_{tot} is close to E_{es} in most cases shown in Supplementary Table S2 and also in many other cases[13,14,42,43].

The most stable structures for the N_2 dimer ($N_2 - N_2$) are the displaced-Parallel (Pd) shape ($E_e = -1.24$ kJ/mol) and the L-shape ($E_e = -1.22$ kJ/mol). In the Pd structure the negatively charged bond-end of one molecule is on top of the positively charged bond-surface of the other molecule, and vice versa. In the L-shape the negatively charged bond-end of one molecule is directly pointing to the positively charged bond-surface of the other molecule. In both Pd and L shapes, the electrostatic energy ($E_{es} = -0.74$ and -0.76 kJ/mol, respectively) is important. In the case of the hetero-molecular interaction between N_2 (which has electrostatically negative bond-ends) and F_2 (which has electrostatically positive bond-ends), a linear structure is the most stable in the potential energy surface ($E_e = -2.24$ kJ/mol) where the key energy contribution is the electrostatic energy ($E_{es} = -2.58$ kJ/mol). In the homo-dimer systems, while E_{es} is important, the dispersion term E_{disp*} related to the van der Waals radius and van der Waals interaction can also be important in determining their structures (see Supplementary Note 2 for the details).

Interactions of the homonuclear diatomic molecules with benzene. The interactions of homonuclear diatomic molecules with benzene (Bz) are shown in Figure 4c. Hobza and coworkers carried out a similar study[44]. Bz has negatively charged electron clouds both above and below the Bz-plane, while being surrounded by positively charged H atoms around the edge. The parallel structure is the most stable ($E_e = -6.3/-5.5$ kJ/mol) for $N_2/^1O_2$, since the electrostatically negative surface of the Bz-plane favorably interacts with the electrostatically positive cylindrical-bond-surface of $N_2/^1O_2$. For the interaction between Bz and F_2/Cl_2 the T-shape-on-bond structure is the most stable ($E_e = -6.0/-12.7$ kJ/mol), as the most electrostatically negative CC aromatic bond of the Bz-plane favorably interacts with an electrostatically positive bond-end of F_2. Based on this information, we can understand the interactions of these diatomic molecules with Bz and further with graphene. In general, for the Bz-A_2 complexes, even though the dispersion energy is dominant in magnitude, the anisotropic charge distribution in A_2 plays an important role in determining the most stable structures (Supplementary Note 3).

We performed SAPT/DFT calculations to decompose the interaction energy into physically meaningful components (Supplementary Table S2). For Bz-N_2, the most stable parallel structure (P) shows strong electrostatic energy ($E_{es} = -4.55$ kJ/mol), while the effective dispersion and exchange energies nearly cancel each other ($E_{disp*} + E_{exch*} = -0.25$ kJ/mol); thus, this structure is electrostatically driven. For Bz-O_2 (singlet), the most stable parallel (P) structure shows strong electrostatic energy (E_{es}: -13.01 kJ/mol), while $E_{disp*} + E_{exch*} + E_{HF}$ (2.55 kJ/mol) is slightly positive; thus, it forms an electrostatically driven structure. For Bz-F_2, the most stable T-shape-on-bond structure (Tb) exhibits a large electrostatic energy ($E_{es} = -5.87$ kJ/mol), while the $E_{disp*} + E_{exch*}$ (4.38 kJ/mol) is positive; as such it forms an electrostatically driven structure. A similar behavior is noted in Bz-Cl_2, but with stronger interaction energy. The most stable Tb structure shows strong electrostatic energy (E_{es}: -13.10 kJ/mol), while the $E_{disp*} + E_{exch*}$ (8.17 kJ/mol) is positive, forming an electrostatically driven structure. In general, for the Bz-A_2 complexes, even though the magnitude of the effective dispersion

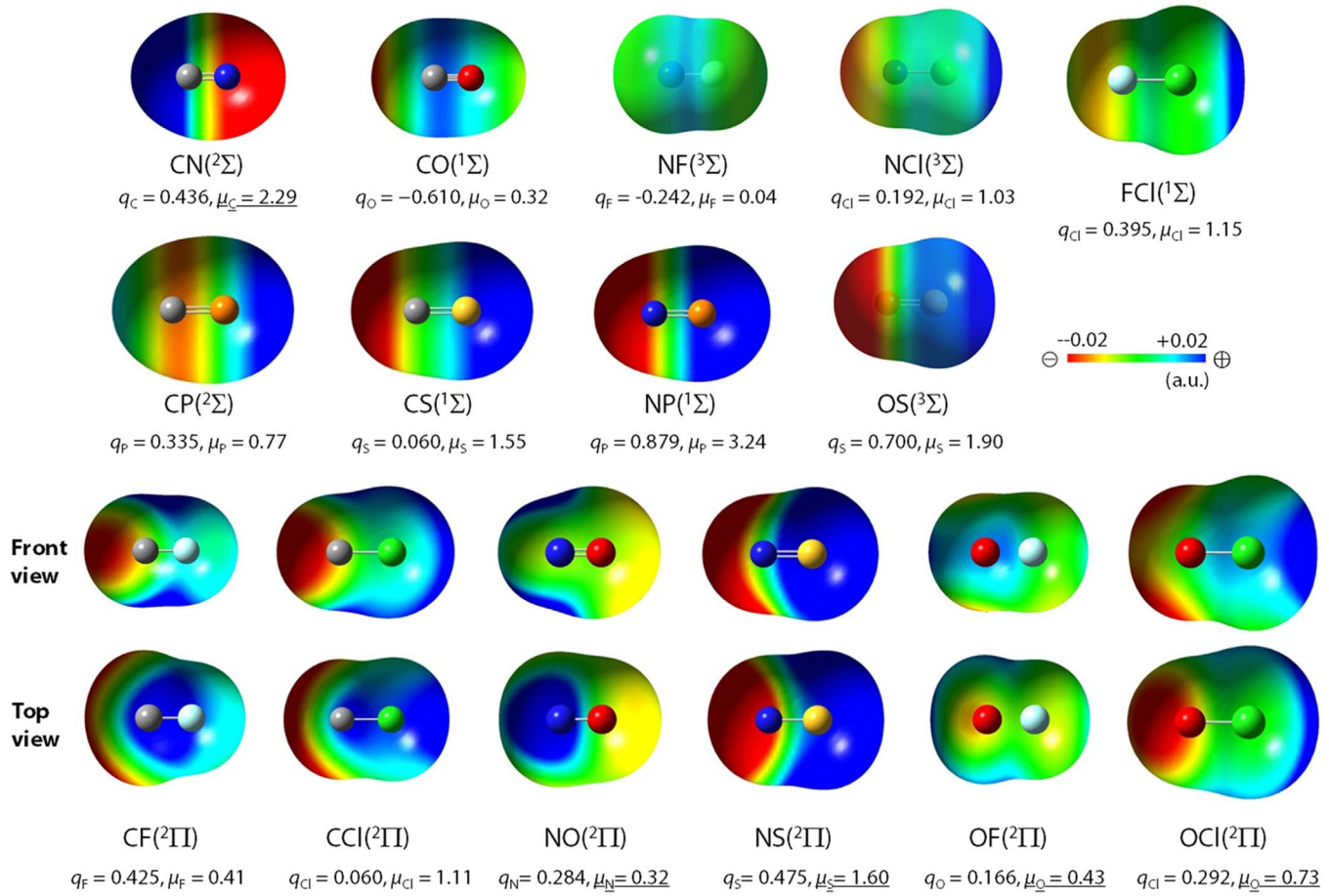

Figure 5 | ESP of heteronuclear diatomic molecules (MP2/aVTZ). q: NBO charge (au), μ_A: dipole moment (debye), where the subscript A designates the atom to which the dipole direction is pointing from the molecular center. The dipole vectors are along the right direction except the left direction of the three cases of CN, NO, and OF (for which the nuclear charge difference between two atoms is only 1).

is very large, the anisotropic charge distribution in A_2 plays a very important role in determining the structures.

Heteronuclear diatomic molecules. The ESP maps for heteronuclear diatomic molecules of nonmetallic elements are computed at MP2/aVTZ level. The charge analysis according to ESP (somewhat different from the NBO charge analysis, for example, as in CO for which the NBO charges give the wrong dipole direction) of heteronuclear diatomic molecules shows: $C^{\delta+}$ $N^{\delta-}$, $C^{\delta-}$ $O^{\delta+}$, $C^{\delta-}$ $F^{\delta+}$, $N^{\delta+}$ $O^{\delta-}$, $N^{\delta-}$ $F^{\delta+}$, $O^{\delta+}$ $F^{\delta-}$, $N^{\delta-}$ $P^{\delta+}$, $O^{\delta-}$ $S^{\delta+}$, $F^{\delta-}$ $Cl^{\delta+}$, $C^{\delta-}$ $P^{\delta+}$, $C^{\delta-}$ $S^{\delta+}$, $C^{\delta-}$ $Cl^{\delta+}$, $N^{\delta-}$ $S^{\delta+}$, $N^{\delta-}$ $Cl^{\delta+}$, and $O^{\delta-}$ $Cl^{\delta+}$ (Figure 5). This result is counterintuitive, since the more electronegative element is positively charged except for a few cases. Therefore, we speculate that the electrons tend to be populated to reduce the electrostatic imbalance, i.e., to neutralize the electrostatical positivess around the nuclei, but not sufficiently. Therefore, the regions around the nuclei with the larger nuclear-charge (i.e., higher electronegativity) tend to be electrostatically positive except for the group I–III elements which tend to be strongly electrostatically positive. Indeed, such a trend holds for almost all the cases of the above hetero-diatomic molecules. As for the three exceptional cases $C^{\delta+}$ $N^{\delta-}$, $N^{\delta+}$ $O^{\delta-}$, and $O^{\delta+}$ $F^{\delta-}$ (three left-top ESP maps in Figure 5), the two nuclear-charges are similar (the nuclear-charge difference is only one). Therefore, their positiveness/negativeness could depend delicately on MOs. CN is isoelectronic to N_2^+, the ionized state of N_2. An electron can be easily detached from the less positively charged nucleus C in CN^- isoelectronic to N_2, which provides the electrostatically positive site for the C atom. The electronic behaviors of NO (isoelectronic to O_2^+) and OF (isoelectronic to F_2^+) can be explained similarly. However, we observe a tendency for diatomic molecules of nonmetals to have opposite atomic charges against those predicted by Pauling's electronegativity when the two elements are at least two groups apart.

Discussion

We analyzed the anisotropic charge distribution and anisotropic van der Waals radii of atoms in diverse diatomic molecules to understand intriguing novel molecular interactions. We scrutinized molecular interactions of various diatomic molecules of Group (IV–VII) elements (which disfavor anionic species) with themselves, a cation(Na^+)/anion(Cl^-), H_2O, and benzene. Though there have been some discussions on such group elements interacting with anionic sites or themselves, the clear understanding was lacking. For accurate description of their subtle interactions, we note that the anisotropy in charge distribution around the atoms which arise from a number of factors including MO, nuclear charge and bond length should be considered. The fundamental understanding of the origin and characteristic features of anisotropic noncovalent interactions could be utilized in novel molecular recognition, assembling, engineering, and dynamical control.

Methods

The ESP at each point in space is defined as in Equation (1), where Z_I and $\mathbf{R}_I$ are the nuclear charge and position, respectively.

$$V(\mathbf{r}) = \sum_I \frac{Z_I}{|\mathbf{r}-\mathbf{R}_I|} - \int \frac{\rho_e(\mathbf{r}')}{|\mathbf{r}-\mathbf{r}'|} d\mathbf{r}' \quad (1)$$

The quadrupole moment Q_{zz} is defined as in Equation (2), which becomes more negative/positive as the electron-population gets contracted/expanded toward the

z-axis (i.e., as the electron-population is more oblated/prolated in the diatomic molecule).

$$Q_{zz} = \int \left(3z^2 - r^2\right) \left[\sum_I Z_I \delta(\mathbf{r} - \mathbf{R}_I) - \rho_e(\mathbf{r})\right] d\mathbf{r} \quad (2)$$

The CCSD(T)/CBS limit (E_{CBS}) of an interaction energy (E) is evaluated based on the extrapolation method[45,46] exploiting that the basis set error in the electron correlation energy is proportional to N^{-3} for the aug-cc-pV*N*Z (aV*N*Z) basis set ($E_{CBS} = [E_N{*}N^3 - E_{N-1}{*}(N-1)^3]/[N^3 - (N-1)^3]$). Here, CCSD(T)/aVTZ and CCSD(T)/aVQZ energies at the CCSD(T)/aVTZ optimized geometries were used for the extrapolation to the CBS limit. Ab initio calculations were carried out using Gaussian [Frisch, M. J. *et al.* Gaussian 09, revision A.02 (Gaussian, Inc., 2009)] and Molpro [Werner, H.-J. *et al.* Molpro quantum chemistry package, version 2012.1, http://www.molpro.net./ (2012) (date of access: 01/06/2012)] packages.

1. Zhang, S. Fabrication of novel biomaterials through molecular self-assembly. *Nature Biotechnol.* **21**, 1171–1178 (2003).
2. Hoeben, F. J. M., Jonkheijm, P., Meijer, E. W. & Schenning, A. P. H. J. About supramolecular assemblies of π-conjugated systems. *Chem. Rev.* **105**, 1491–1546 (2005).
3. Lee, J. Y. *et al.* Near-field focusing and magnification through self-assembled nanoscale spherical lenses. *Nature* **460**, 498–501 (2009).
4. Salonen, L. M., Ellermann, M. & Diederich, F. Aromatic rings in chemical and biological recognition: energetics and structures. *Angew. Chem. Int. Ed.* **50**, 4808–4842 (2011).
5. Hobza, P. & Muller-Dethlefs, K. Non-covalent interactions: theory and experiment (Royal Soc. Chem. 2009).
6. Georgakilas, V. *et al.* Functionalization of Graphene: Covalent and noncovalent approaches, derivatives and applications. *Chem. Rev.* **112**, 6156–6214 (2012).
7. Singh, N. J., Lee, H. M., Hwang, I.-C., & Kim, K. S. Designing ionophores and molecular nanotubes based on molecular recognition. *Supramol. Chem.* **19**, 321–332 (2007).
8. Mingos, D. M. *Supramolecular assembly via hydrogen bonds II.* (Springer-Verlag, 2004).
9. Grabowski, S. J. Hydrogen bonding - new insights. (Springer, 2006).
10. Lee, H. M. *et al.* Comparison of cationic, anionic and neutral hydrogen bonded dimers. *Phys. Chem. Chem. Phys.* **12**, 6278–6287 (2010).
11. Riley, K. E. & Hobza, P. On the importance and origin of aromatic interactions in chemistry and biodisciplines. *Acc. Chem. Res.* **46**, 927–936 (2013).
12. Sherrill, C. D. Energy component analysis of π Interactions. *Acc. Chem. Res.* **46**, 1020–1028 (2013).
13. Singh, N. J., Min, S. K., Kim, D. Y. & Kim, K. S. Comprehensive energy analysis for various types of pi-interaction. *J. Chem. Theor. Comput.* **5**, 515–529 (2009).
14. Kim, K. S., Tarakeshwar, P. & Lee, J. Y. Molecular clusters of pi-systems: theoretical studies of structures, spectra and origin of interaction energies. *Chem. Rev.* **100**, 4145–4186 (2000).
15. Mahavevi, A. S. & Sastry, G. N. Cation-π Interaction: Its role and relevance in chemistry, biology, and material science. *Chem. Rev.* **113**, 2100–2138 (2013).
16. Fourmigue, M. & Batail, P. Activation of hydrogen- and halogen-bonding interactions in tetrathiafulvalene-based crystalline molecular conductors. *Chem. Rev.* **104**, 5379–5418 (2004).
17. Metrangolo, P., Neukirch, H., Pilati, T. & Resnati, G. Halogen bonding based recognition processes: a world parallel to hydrogen bonding. *Acc. Chem. Res.* **38**, 386–395 (2005).
18. Sun, A., Lauher, J. W. & Gorof, N. S. Preparation of poly(diiodoacetylene), an ordered conjugated polymer of carbon and iodine. *Science* **312**, 1030–1034 (2006).
19. Metrangolo, P. & Resnati, G. Halogen versus hydrogen. *Science* **321**, 918–919 (2008).
20. Riley, K. E. & Hobza, P. Investigations into the nature of halogen bonding including symmetry adapted perturbation theory analyses. *J. Chem. Theory Comput.* **4**, 232–242 (2008).
21. Politzer, P., Murray, J. S. & Clark, T. Halogen bonding: an electrostatically driven highly directional noncovalent interaction. *Phys. Chem. Chem. Phys.* **12**, 7748–7757 (2010).
22. Kerdawy, A. E. *et al.* Directional noncovalent interactions: repulsion and dispersion. *J. Chem. Theory. Comput.* **9**, 2264–2275 (2013).
23. Clark, T., Hennemann, M., Murray, J. S. & Politzer, P. Halogen bonding: the σ-hole. *J. Mol. Model.* **13**, 291–296 (2007).
24. Mohajeri, A., Pakiari, A. H. & Bagheri, N. Theoretical studies on the nature of bonding in σ-hole complexes. *Chem. Phys. Lett.* **467**, 393–397 (2009).
25. Murray, J. S., Lane, P., Clark, T., Riley, K. E. & Politzer, P. σ-Holes, π-holes and electrostatically driven interactions. *J. Mol. Mod.* **18**, 541–548 (2012).
26. Clark, T. σ-Holes. *WIREs Comput. Mol. Sci.* **3**, 13–20 (2013).
27. Politzer, P., Murray, J. S. & Clark, T. Halogen bonding and other σ-hole interactions: a perspective. *Phys. Chem. Chem. Phys.* **15**, 11178–11189 (2013).
28. Sedlak, R., Deepa, P. & Hobza, P. Why is the L-shaped structure of $X_2\cdots X_2$ (X = F, Cl, Br, I) complexes more stable than other structures? *J. Phys. Chem. A* **118**, 3846–3855 (2014).
29. Jones, Jr, M. & Fleming, S. A. Organic chemistry, 5th ed. (W. W. Norton and Company, 2014).
30. Duarte, D. J. R., Angelina, E. L. & Peruchena, N. M. On the strength of the halogen bonds: mutual penetration, atomic quadrupole moment and Laplacian distribution of the charge density analyses. *Comput. Theor. Chem.* **998**, 164–172 (2012).
31. Atkins, P. & de Paula, J. Atkins' physical chemistry, 8th ed. (W. H. Freeman and Company, 2006).
32. Kim, H. G. *et al.* An Electrochemically controllable nanomechanical molecular system utilizing edge-to-face and face-to-face aromatic interacions. *Org. Lett.* **4**, 3971–3974 (2002).
33. Baerends, E. J., Gritsenko, O. V. & van Meer, R. The Kohn-Sham gap, the fundamental gap and the optical gap: the physical meaning of occupied and virtual Kohn-Sham orbital energies. *Phys. Chem. Chem. Phys.* **15**, 16408–16425 (2013).
34. Gans, W. & Boeyens, J. C. A. Intermolecular interactions. (Plenum Press, New York, 1988).
35. Leszczynski, J. & Shukla, M. Practical aspects of computational chemistry: methods, concepts and applications. (Springer, New York, 2009).
36. Bui, T. T. T., Dahaoui, S., Lecomte, C., Desiraju, G. R. & Espinosa, E. The nature of halogen...halogen interactions: a model derived from experimental charge-density analysis. *Angew. Chem. Int. Ed.*, **48**, 3838–3841 (2009).
37. Lee, H. M., Suh, S. B., Lee, J. Y., Tarakeshwar, P. & Kim, K. S. Structures, energies, vibrational spectra, and electronic properties of water monomer to decamer. *J. Chem. Phys.* **112**, 9759–9772 (2000).
38. Du, Q., Superfine, R., Freysz, E. & Shen, Y. R. Vibrational spectroscopy of water at the vapor/water interface. *Phys. Rev. Lett.* **70**, 2313–2316 (1993).
39. Du, Q., Freysz, E. & Shen, Y. R. Surface vibrational spectroscopic studies of hydrogen bonding and hydrophobicity. *Science* **264**, 826–828 (1994).
40. Jeziorski, B., Moszynski, R. & Szalewicz, K. Perturbation theory approach to intermolecular potential energy surfaces of van der Waals complexes. *Chem. Rev.* **94**, 1887–1930 (1994).
41. Szalewicz, K. Symmetry-adapted perturbation theory of intermolecular forces. *WIREs Comput. Mol. Sci.* **2**, 254–272 (2012).
42. Lee, E. C. *et al.* Substituent effects on the edge-to-face aromatic interactions. *J. Am. Chem. Soc.* **127**, 4530–4537 (2005).
43. Lee, E. C. *et al.* Understanding of Assembly Phenomena by Aromatic-aromatic interactions: benzene dimer and the substituted systems. *J. Phys. Chem. A* **111**, 3446–3457 (2007).
44. Munusamy, E., Sedlak, R. & Hobza, P. On the nature of the stabilization of benzene…dihalogen and benzene…dinitrogen complexes: CCSD(T)/CBS and DFT-SAPT calculations. *ChemPhysChem* **12**, 3253–3261 (2011).
45. Helgaker, T., Klopper, W., Koch, H. & Noga, J. Basis-set convergence of correlated calculations on water. *J. Chem. Phys.* **106**, 9639–9648 (1997).
46. Min, S. K. *et al.* Complete basis set limit of ab initio binding energies and geometrical parameters for various typical types of complexes. *J. Comput. Chem.* **29**, 1208–1221 (2008).

Acknowledgments

This work was supported by NRF (National Honor Scientist Program: 2010-0020414) and KISTI (KSC-2011-G3-02).

Author contributions

H.K. discovered the intriguing features and started the project. D.V.D. performed refined calculations. M.V.M. assisted in calculations. H.K., W.J.C. and K.S.K. analyzed the data and wrote the manuscript. H.K. and D.V.D. contributed equally and are co-first authors.

Additional information

Supplementary information accompanies this paper at http://www.nature.com/scientificreports

Competing financial interests: The authors declare no competing financial interests.

How to cite this article: Kim, H., Doan, V.D., Cho, W.J., Madhav, M.V. & Kim, K.S. Anisotropic Charge Distribution and Anisotropic van der Waals Radius Leading to Intriguing Anisotropic Noncovalent Interactions. *Sci. Rep.* **4**, 5826; DOI:10.1038/srep05826 (2014).